

Gamma Rays from Top-Mediated Dark Matter Annihilations

C. B. Jackson^a, G  raldine Servant^{b,c,d}, Gabe Shaughnessy^e,
Tim M.P. Tait^f, and Marco Taoso^{d,g}

^a*University of Texas at Arlington, Arlington, TX 76019 USA*

^b*CERN Physics Department, Theory Division, CH-1211 Geneva 23, Switzerland*

^c*ICREA at IFAE, Universitat Aut  noma de Barcelona, 08193 Bellaterra, Barcelona, Spain*

^d*Institut de Physique Th  orique, CEA/Saclay, F-91191 Gif-sur-Yvette C  dex, France*

^e*Department of Physics, University of Wisconsin, Madison, WI 53706 USA*

^f*Department of Physics & Astronomy, University of California, Irvine, CA 92697 USA*

^g*Department of Physics & Astronomy, University of British Columbia, Vancouver, BC V6T 1Z1 Canada*

geraldine.servant@cern.ch, chris@uta.edu,
gshau@hep.wisc.edu, ttait@uci.edu, marco.taoso@cea.fr

Abstract

Lines in the energy spectrum of gamma rays are a fascinating experimental signal, which are often considered “smoking gun” evidence of dark matter annihilation. The current generation of gamma ray observatories are currently closing in on parameter space of great interest in the context of dark matter which is a thermal relic. We consider theories in which the dark matter’s primary connection to the Standard Model is via the top quark, realizing strong gamma ray lines consistent with a thermal relic through the forbidden channel mechanism proposed in the Higgs in Space Model. We consider realistic UV-completions of the Higgs in Space and related theories, and show that a rich structure of observable gamma ray lines is consistent with a thermal relic as well as constraints from dark matter searches and the LHC. Particular attention is paid to the one loop contributions to the continuum gamma rays, which can easily swamp the line signals in some cases, and have been largely overlooked in previous literature.

1 Introduction

The existence of nonbaryonic dark matter is well established, but there is still no clue as to its particle identity, and no indication as to what interactions beyond gravitational it experiences. In order to place dark matter in context within the Standard Model or its extensions, observation of dark matter interacting through something other than gravity will be required. There is currently a rich and diverse experimental program searching for dark matter through its direct scattering with nuclei, produced at colliders, or indirectly through its annihilation products.

This last pillar of the searches for dark matter is particularly interesting. Observation of dark matter annihilation would be a clear indication that dark matter has non-gravitational interactions, and (depending on the observations) would help to establish it as a thermal relic. In fact, observations of dwarf spheroidals by the Fermi LAT currently exclude s -wave annihilating thermal relic dark matter with mass below about 50 GeV [1, 2].

An important element in the indirect search for dark matter is the search for lines in the energy spectrum of gamma rays. Such features occur when dark matter annihilates into a two-particle final state, with one of the particles a photon. Since dark matter must be electrically neutral (to good approximation [3]), such a signal is typically expected to be rather smaller than the expected annihilation cross section of a thermal relic, $\langle\sigma v\rangle \sim 3 \times 10^{-26} \text{ cm}^2/\text{s}$ (with mild dependence on the dark matter mass [4]). Nonetheless, such a gamma ray line is a very distinctive signal, unlikely to be faked by astrophysical backgrounds. In preparation for further data from Fermi, as well as new data sets from H.E.S.S., CTA, and other future gamma ray observatories, it is worthwhile to explore theories which would be expected to result in a prominent line signal.

Typically, there is some tension between the need to have a large loop level line signal without ending up with a large annihilation cross section into continuum photons, which could either swamp the line signal, or would over-saturate the thermal cross section. An early step in this direction was the “Higgs in Space” model [5], which was inspired by models of dark matter in the setting of warped extra dimensional GUTs [6, 7], and had a Dirac fermion dark matter which annihilated through a Z' which coupled preferentially to top quarks. By annihilating into top quarks, one could arrange for a thermal relic with masses slightly below the top mass which allowed for efficient annihilation in the early universe, but suppressed continuum annihilation in cold structures such as galaxies today.

Ingredients such as s -channel resonant annihilation and forbidden channels in the final state have received much attention recently [8], largely in response to the reported excess of gamma rays around ~ 130 GeV originating close to the galactic center in the Fermi LAT data [9–12]. While interest was inflamed by a subdominant signal at around 115 GeV consistent with an additional annihilation channel into γZ [11, 13, 14], peculiar features such as an excess of photons at the same energy from the Earth’s limb [11, 15, 16] could point to an instrumental origin for the feature. While many of the constructions we consider could potentially explain the Fermi signal should it turn out to actually be dark matter, we remain agnostic about its origin and consider theories with enhanced lines in general.

In a previous paper [18], we considered the forbidden channel mechanism in the context of dark matter which annihilates through exotic states with only weak connection to the Standard Model itself. We made the important observation that for this class of models,

the one-loop continuum annihilation channels cannot typically be ignored, and often play an important role in determining both the observability of a line signal as well as the relic density. In the current article, we revisit models closer in spirit to the Higgs in Space, where the role of the SM-charged mediator is once again played by the top quark. We consider UV-complete models, and derive predictions for gamma ray lines, as well as conditions for a thermal relic, constraints from direct detection, precision measurements, and the LHC.

Our article is outlined as follows: in Section 2 we set up the basic module containing the necessary ingredients, building on the experience of Ref. [18]. In Section 3, we compute the constraints from precision measurements and the observed properties of the newly discovered Higgs boson, which help narrow down the viable parameter space, as well as direct constraints from LHC searches. In Section 4, we compute the rates for dark matter annihilation at one loop, including contributions to the continuum gammas, gamma ray lines, and the relic density. Finally, we conclude in Section 6. The appendices contain detailed expressions for effective vertices at one loop, complementing those already presented in Ref. [18].

2 Top as a Messenger to Dark Matter

The basic set-up builds on the models explored in [18]: the dark matter is a Dirac¹ fermion ν with no SM gauge interactions, but charged under a $U(1)'$ symmetry². The SM (with the subtle exception of the top quark as outlined below) is uncharged under the $U(1)'$, resulting in very weak bounds from precision measurements [19]. The $U(1)'$ is higgsed by a scalar particle, resulting in a massive Z' vector boson and a Higgs-like state Φ (which is not to be confused the SM Higgs boson h). For simplicity, we assume that any kinetic mixing between the $U(1)'$ and the SM hypercharge interaction is small enough to be ignored. Both the Z' and Φ can act as mediators between the dark matter and some additional fermions ψ which are charged under the Standard Model. In Ref. [18], we restricted our attention to the case where ψ was electroweakly- but not color-charged; this avoided constraints from the LHC and prevented annihilation into gluons. In this article, we consider the case where the role of ψ is played by an extended top sector.

We denote by \hat{t}_R the field which will largely become the right-handed top quark, uncharged under the $U(1)'$ and in the $(3, 1, 2/3)$ representation under the SM ($SU(3)$, $SU(2)$, $U(1)$) symmetries. Similarly, \hat{Q}_3 is the usual left-handed quark doublet for the third generation. The additional fermions $\psi_{L,R}$ have equal charges under $U(1)'$ and are charged as $(3, 1, 2/3)$ under the SM. By introducing a vector-like pair of ψ fields, we avoid disrupting the cancellation of any of the purely SM anomalies. The ψ fields are also vector-like under $U(1)'$, and thus no mixed SM- $U(1)'$ anomalies are generated. The last remaining potential gauge anomalies (depending on the charges of ν_L and ν_R) are $U(1)'$ -gravity² or $U(1)'^3$, and can be arranged by including additional SM singlet fermions which are charged under $U(1)'$. When present, these fermions are essentially irrelevant for the phenomena of interest to us, and we will ignore them in the subsequent discussion.

¹One could engineer Majorana dark matter, by involving another fermion charged under $U(1)'$, but this would require ν - Z' axial interactions, and would generally lead to a large annihilation into gg [18].

²We consider variations where the dark matter ν either has vector-like $U(1)'$ interactions, in which case one can write down a gauge-invariant mass, or have chiral interactions, in which case the mass for the dark matter will have to be generated by the $U(1)'$ -breaking VEV.

The terms responsible for top- ψ mixing are structurally reminiscent of top-seesaw models [20–23],

$$\mathcal{L}_{\text{mass}} = yH\bar{Q}_3\hat{t}_R + \mu\bar{\psi}_L\psi_R + Y\Phi\bar{\psi}_L\hat{t}_R \quad (1)$$

where H is the SM Higgs doublet, y and Y are dimensionless couplings, and μ is a gauge-invariant mass term for ψ . We define mass eigenstates t and T :

$$\begin{pmatrix} t_{R/L} \\ T_{R/L} \end{pmatrix} = \begin{pmatrix} -\sin\theta_{R/L} & \cos\theta_{R/L} \\ \cos\theta_{R/L} & \sin\theta_{R/L} \end{pmatrix} \begin{pmatrix} \hat{t}_{R/L} \\ \Psi_{R/L} \end{pmatrix}, \quad (2)$$

with eigenmasses,

$$M_{t/T}^2 = \frac{1}{2} \left[\mu^2 + y^2\langle H^2 \rangle + Y^2\langle \Phi^2 \rangle \mp \sqrt{-4\mu^2 y^2\langle H^2 \rangle + (\mu^2 + y^2\langle H^2 \rangle + Y^2\langle \Phi^2 \rangle)^2} \right], \quad (3)$$

and mixing angles θ_R and θ_L given by,

$$\begin{aligned} \tan\theta_R &= \frac{\mu^2 - y^2\langle H^2 \rangle - Y^2\langle \Phi^2 \rangle + \sqrt{-4\mu^2 y^2\langle H^2 \rangle + (\mu^2 + y^2\langle H^2 \rangle + Y^2\langle \Phi^2 \rangle)^2}}{2\mu Y\langle \Phi \rangle} \\ \tan\theta_L &= \frac{\mu^2 - y^2\langle H^2 \rangle + Y^2\langle \Phi^2 \rangle + \sqrt{-4\mu^2 y^2\langle H^2 \rangle + (\mu^2 + y^2\langle H^2 \rangle + Y^2\langle \Phi^2 \rangle)^2}}{2y\langle H \rangle Y\langle \Phi \rangle}. \end{aligned} \quad (4)$$

We identify the lighter mass eigenstate with the top quark of mass $m_t \simeq 174$ GeV, leaving two free parameters which we choose to be $y\langle H \rangle$ and $Y\langle \Phi \rangle$. Imposing the top mass constraint, μ is given by,

$$\mu^2 = m_t^2 \frac{m_t^2 - y^2\langle H^2 \rangle - Y^2\langle \Phi^2 \rangle}{m_t^2 - y^2\langle H^2 \rangle} \quad (5)$$

and M_T is determined. We show the contours of μ , M_T , $\cos\theta_R$ and $\cos\theta_L$ in Fig. 1. It is worth noting that in the limit $Y\langle \Phi \rangle \rightarrow 0$, the mixing angles do not go to zero (unless one also requires $y\langle H \rangle \rightarrow m_t$). For a fixed $y\langle H \rangle \neq m_t$, the limit $Y\langle \Phi \rangle \rightarrow 0$ necessarily implies $\mu \rightarrow m_t$ in order to keep the lightest mass eigenstate at $m_t = 174$ GeV. In addition, in the SM-like regime where $c_R, c_L \ll 1$ and the second mass eigenstate is very heavy is obtained for $Y\langle \Phi \rangle, \mu \rightarrow \infty$. Finally, the case where $y\langle H \rangle \sim m_t$ and $M_T \gg m_t$ corresponds to a value of $Y\langle \Phi \rangle$ which is parametrically smaller than M_T itself.

In the mass basis one has diagonal interactions of t and T as well as mixed t - T interactions,

$$\begin{aligned} \mathcal{L} &= i\bar{t}\not{D}_t t + i\bar{T}\not{D}_T T + \frac{g}{\sqrt{2}}(c_L\bar{T} - s_L\bar{t})\gamma^\mu W_\mu P_L b + h.c. \\ &+ s_L c_L [g_{t_R}^Z - g_{t_L}^Z] \bar{T}\gamma^\mu Z_\mu P_L t + h.c. \\ &+ \bar{T}\gamma^\mu \hat{Z}'_\mu g_\psi^{\hat{Z}'} (s_L c_L P_L + s_R c_R P_R) t + h.c. \\ &+ y s_L s_R h \bar{t} t + y c_L c_R h \bar{T} T - y h \bar{t} (c_R s_L P_R + c_L s_R P_L) T + h.c. \\ &- Y c_L s_R \varphi \bar{t} t + Y s_L c_R \varphi \bar{T} T + Y \varphi \bar{t} (c_L c_R P_R - s_L s_R P_L) T + h.c. \end{aligned} \quad (6)$$

where

$$D_{t_\mu} = \partial_\mu - i \left[(g_{t_R}^Z c_L^2 + g_{t_L}^Z s_L^2) P_L + g_{t_R}^Z P_R \right] Z_\mu - i g_\psi^{\hat{Z}'} (c_R^2 P_R + c_L^2 P_L) \hat{Z}'_\mu - i g_{t_R}^\gamma A_\mu \quad (7)$$

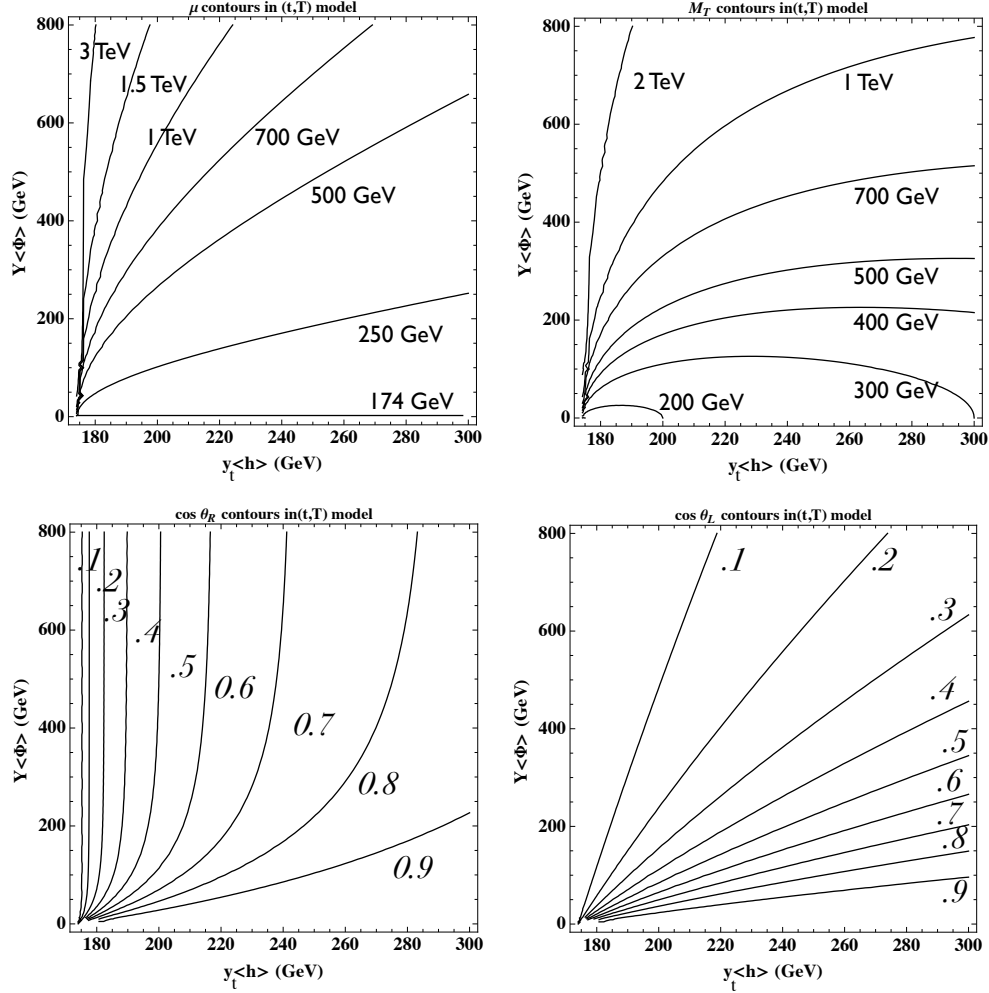


Figure 1: Contours of μ , M_T , $\cos \theta_R$ and $\cos \theta_L$ in the top partner model.

and,

$$D_{T\mu} = \partial_\mu - i \left[(g_{t_R}^Z s_L^2 + g_{t_L}^Z c_L^2) P_L + g_{t_R}^Z P_R \right] Z_\mu - i g_\psi^{\hat{Z}'} (s_R^2 P_R + s_L^2 P_L) \hat{Z}'_\mu - i g_{t_R}^\gamma A_\mu \quad (8)$$

with $g_{t_R}^\gamma = 2e/3$, $g_{t_{R/L}}^Z = e \cos \theta_W^{-1} \sin \theta_W^{-1} (T_3 - (2e/3) \sin^2 \theta_W)$ and $g = e/\sin \theta_W$ the usual gauge couplings. In addition, both t and T have the usual diagonal color-triplet couplings to gluons, as enforced by $SU(3)$ gauge invariance. We have introduced the short-hand notation $c_L \equiv \cos \theta_L$, $s_R \equiv \sin \theta_R$, etc.

3 Precision and LHC Constraints

Before turning to the annihilation cross sections and resulting line signals, we examine the constraints on the parameter space from precision measurements, LHC searches and direct DM experiments.

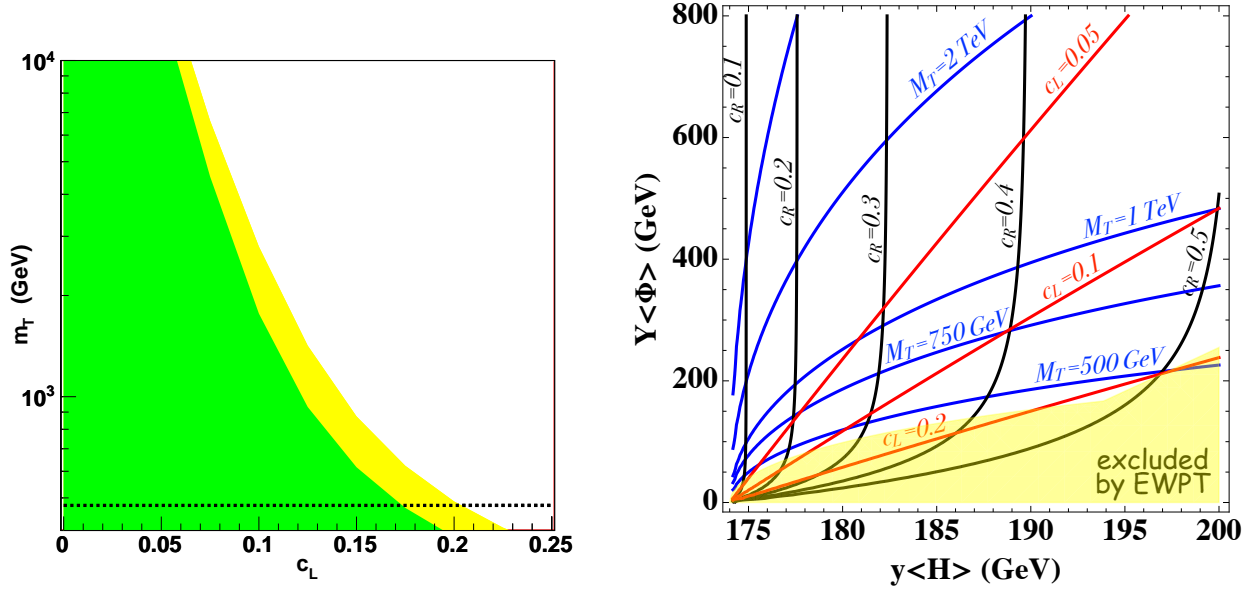


Figure 2: (a) Region of the parameter space of M_T and c_L consistent with precision electroweak data at 1σ (green region) and 95% confidence level (yellow region). Also shown is the approximate lower bound on M_T from null LHC searches (dashed line); (b) Contour plots for c_L, c_R and M_T in the $(\langle yH \rangle, \langle Y\Phi \rangle)$ plane where the yellow region is excluded by EW data.

3.1 Oblique Corrections

As a consequence of mixing with T , the $Z\text{-}\bar{t}_L\text{-}t_L$ and $W\text{-}\bar{t}_L\text{-}b_L$ EW interactions of the top quark are modified with respect to the Standard Model; these deviations are small in the unmixed limit of $c_L \rightarrow 0$. Because of the modified EW interactions of top, as well as diagrams containing the partner quark T explicitly, there are oblique contributions to the precision electroweak observables encapsulated by the Peskin-Takeuchi parameters [24] which provide bounds on the mixing parameter c_L and M_T . The relevant corrections were computed in Refs. [23, 25], where it was found that ΔS and ΔU are very small, and the dominant constraint is from ΔT ,

$$\Delta T = T_{SM} \times c_L^2 \left(-(1 + s_L^2) + c_L^2 r + 2s_L^2 \frac{r}{(r-1)} \log r \right) \quad (9)$$

where,

$$r \equiv \frac{m_T^2}{m_t^2}, \text{ and } T_{SM} = \frac{3}{16\pi s_W^2} \frac{m_t^2}{M_W^2} \simeq 1.19. \quad (10)$$

For a Higgs mass of $m_h = 125.7 \pm 0.4$ GeV, a global fit to the electroweak data restricts $\Delta T \leq 0.14$ (0.10) for $\Delta S \simeq \Delta U \simeq 0$ at the 95% (68%) confidence level [26]. For a fixed value of the mixing c_L , this corresponds to an upper bound on M_T . The constrained region is plotted in Fig. 2(a), and indicates that for $c_L \sim 0.1$, masses $M_T \leq 3$ TeV are consistent with precision measurements. Also shown on the figure is the line corresponding to $M_T \geq$



Figure 3: h and φ production by gluon fusion and their decay into $\gamma\gamma$.

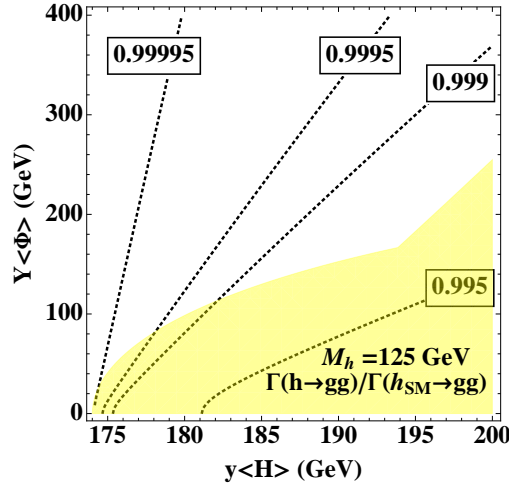


Figure 4: Contours for $\Gamma_{h \rightarrow gg} / \Gamma_{h \rightarrow gg}^{SM}$. The yellow region is excluded by precision electroweak measurements.

475 GeV, which is a conservative estimate for the lower bound on the mass of the T quark based on a collider searches (see below).

We show in Fig. 2(b) the contour plots for c_L, c_R and M_T in the parameter space of $y\langle H \rangle$ and $Y\langle \Phi \rangle$, with the region excluded by precision measurements overlaid. In the allowed region, c_L is smaller than ~ 0.2 , but c_R may still be sizable provided T is not too heavy.

3.2 Constraints from Higgs Measurements

In addition, there can be constraints on c_L and c_R from production of the newly discovered Higgs boson [29] at the LHC, which receives modifications due to the shift in the top coupling to the Higgs, as well as corrections from the T quark itself, which contributes to Higgs interactions with gluons and photons (see Fig. 3). However, in the region consistent with precision electroweak constraints, Higgs phenomenology remains almost very close to Standard Model-like at the LHC. For example, the corrections to $h \rightarrow gg$ (which also characterize the shift in inclusive Higgs production) are,

$$\Gamma_{h \rightarrow gg} \propto \left| \frac{s_L s_R F_{1/2}(\tau_t)}{m_t/v} + \frac{c_L c_R F_{1/2}(\tau_T)}{m_T/v} \right|^2 \propto \left| \frac{F_{1/2}(\tau_t)}{m_t/v} \right|^2, \quad (11)$$

where the function $F_{1/2}$ of $\tau_q \equiv m_h^2/(4m_q^2)$ can be found in Ref. [30]. As illustrated in Fig. 4, these are much less than 1% deviations for the parameter space of interest. Such

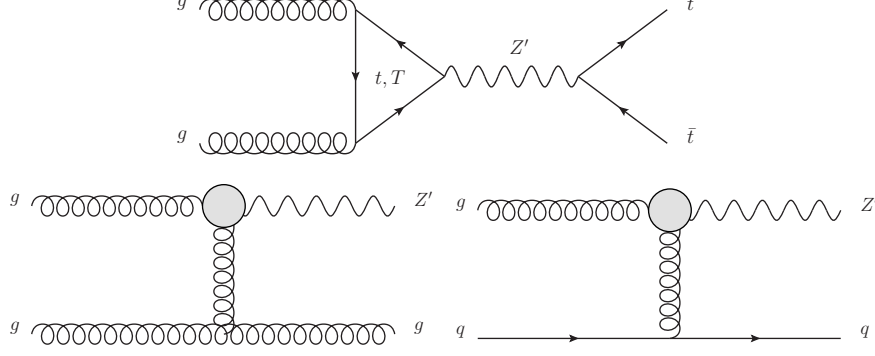


Figure 5: Production diagrams for Z' through its induced coupling to gluons.

tiny deviations might be measurable at a future linear collider and/or Higgs factory, but are unlikely to be accessible at the LHC. Similarly, the correction to $h \rightarrow \gamma\gamma$ is likely to be even smaller since it is dominantly mediated via a W loop, and would be extremely difficult to detect.

One could also search for the Φ boson, which, once produced, would decay via its mixing with the Higgs. However, the t and T loops contributing to Φ production at the LHC almost cancel since $\tan \theta_R / \tan \theta_L \equiv m_t / m_T$, and

$$\Gamma_{\varphi \rightarrow gg} \propto \left| -\frac{c_L s_R F_{1/2}(\tau_t)}{m_t/v} + \frac{s_L c_R F_{1/2}(\tau_T)}{m_T/v} \right|^2 \propto \frac{c_L^2 c_R s_R}{m_t} |F_{1/2}(\tau_t)|^2 \left| 1 - \frac{F_{1/2}(\tau_T)}{F_{1/2}(\tau_t)} \right|^2, \quad (12)$$

resulting in the production rate of Φ being very suppressed.

3.3 Constraints from LHC Searches

The primary constraints from the LHC are from the null searches for exotic quarks such as our T . As a vector-like quark which mixes with the top, the primary decays are expected to be: $T \rightarrow Wb$, $T \rightarrow Zt$, and $T \rightarrow ht$. In addition, if either Φ or Z' are light enough, one could have decays into either one of them plus a top quark. Null searches for the Wb , Zt , and ht channels at the LHC result in a conservative (in the sense that larger masses are permitted for any configuration of branching ratios) bound of $M_T \geq 475$ GeV [27, 28]. In the case where T decays entirely into th , the current bound derived from ATLAS data is 425 GeV [27].

In addition, there are constraints on various types of Z' bosons that may be inferred from LHC searches. The primary interaction of the Z' with the Standard Model is with top quarks. As we shall see, the result is suppressed production cross sections which are generically safe from LHC bounds.

Given the large coupling to top quarks, the dominant Z' production is via gluon fusion through a top loop, as in Figure 5. Detailed expressions for the effective Z' - g - g vertex are provided in Appendix B. The Z' can subsequently decay into $\nu\bar{\nu}$ leading to a missing energy signature, or back into top quarks leading to a resonance in the invariant mass distribution of $t\bar{t}$ pairs. An interesting feature of this signal arises because the Landau-Yang theorem [31]

insures that the amplitude must vanish when the Z' is on-shell. As a result, the signal is much smaller than one might naively expect, and would have an interesting shape around the Z' resonance if it were visible and the Z' width were large enough to permit it to be experimentally mapped out. However, from the point of view of constraining the parameters, one can derive more stringent bounds by considering the process where one of the initial gluons is highly off-shell, resulting in a final state consisting of the Z' and an additional hadronic jet (and after the Z' decays to $t\bar{t}$ leads to a $t\bar{t}j$ signature).

The choice of p_T cut on the associated jet can be optimized based on the need to pull one of the initial gluons off-shell so that the Z' production rate escapes from the Landau-Yang suppression, while at the same time not choosing a cut so stringent as to result in a large suppression from the parton distribution functions. Fully optimizing the search cuts is beyond the scope of this work, but for a choice of $p_T > 30$ GeV, large enough to suppress the $t\bar{t}$ background and such that collinear logarithms do not spoil perturbation theory, we find that even for large couplings, the deviation at $\sqrt{s} = 8$ TeV is never more than about 0.1% of the SM $t\bar{t}j$ rate³, with the largest potential deviations occurring when the Z' mass is just above the $t\bar{t}$ decay threshold. For larger values of the p_T cut, the deviation is even smaller. Such deviations are well within the uncertainties in the SM rate from theoretical uncertainties such as the gluon parton flux and scale variation, and thus will be very difficult to extract from the background. This situation is essentially unchanged at $\sqrt{s} = 14$ TeV.

When the Z' decays directly into dark matter, it produces a dark matter mono-jet signature [33]. For very heavy Z' 's, well-represented by a contact interaction, the current LHC bounds are a factor of few too weak to bound our construction [34], but future prospects in this channel would appear to be good. As the Z' gets lighter and is no longer well-approximated by a contact interaction, these bounds are typically somewhat relaxed [35].

The Z' could also be produced through its induced electroweak interactions, through processes such as $q\bar{q} \rightarrow V^* \rightarrow Z'V'$ (where $V, V' = \gamma, Z$), which was considered in Ref. [36] in the context of the Fermi 130 GeV line feature. For Z' - Z - γ couplings large enough to explain the Fermi feature, the LHC can provide useful bounds (though it is somewhat questionable whether such large effective interactions are consistent with a perturbative UV complete theory) in the regime of weak DM- Z' couplings, but in our construction the effective vertex is small enough that there is essentially no useful bound from this channel, even for very light Z' 's.

A Z' with large coupling to top quarks can also be produced as radiation from a $t\bar{t}$ pair through processes such as $gg \rightarrow t\bar{t}Z'$. Its subsequent decay into dark matter leads to a top pair plus missing energy signature [37], or it can decay back into top quarks leading to a four top final state [38–41]. For either process, the rate is modest because of the phase space suppression and is unlikely to be a serious constraint from current LHC data. However, prospects are good for observation at higher energy LHC running.

3.4 Constraints from Direct Detection

For low Z' masses, constraints from null results of direct searches for dark matter (e.g. from Xenon-100 [42]) can be potentially rather strong. In particular, it implies a bound on the

³When the Z' can decay both into $\nu\bar{\nu}$ and $t\bar{t}$, the branching fraction for $Z' \rightarrow t\bar{t}$ is less than 10^{-2} , since the top coupling is suppressed by c_R^2 compared to the ν coupling.

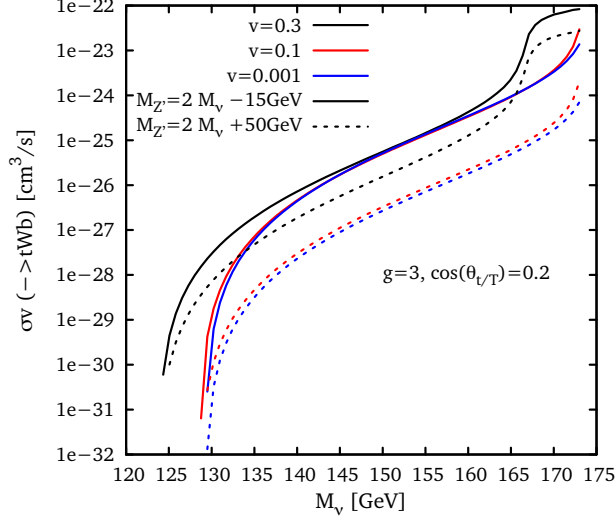


Figure 6: Cross section for annihilation into the 3-body final state tWb for several values of the relative velocity v and $M_{Z'}$ mass, as indicated. We have set $c_L = c_R = 0.2$ for simplicity.

degree of kinetic mixing between the Z and Z' , since that parameter controls the coupling to light quarks⁴. As the direct scattering of ν with nuclei is entirely on protons rather than neutrons, the Xenon-100 bounds (which assume equal scattering with both protons and neutrons) require $\sigma_{p\nu} \lesssim 3 \times 10^{-44} \text{ cm}^2$, corresponding to the restriction $\eta \times g_{Z'} \lesssim 10^{-3}$ [5], where η is the coefficient of the $F_Y^{\mu\nu} F'_{\mu\nu}$ term in the effective action.

In principle, η is a free parameter which is additively renormalized by loops of the t and T quarks. If the $U(1)'$ is embedded in a non-Abelian symmetry, it will naturally vanish at the scale at which that symmetry breaks down to $U(1)'$ (which acts as a UV-cut-off on the log divergence present in the current framework). Its natural value thus depends on both the Z' gauge coupling and the symmetry-breaking scale. For the parameters of interest to us, we find $\eta/g_{Z'} \lesssim \mathcal{O}(10^{-3})$, and thus consistency with the direct bounds requires at most very modest tuning of η .

3.5 Flavor Considerations

Finally, we should mention the possibility of flavor violation. We have chosen to identify the SM quark with which the messengers $\psi_{L,R}$ mix as the top quark, but there are no symmetries that prevent similar mixing terms with the up and charm quarks. Indeed, the CKM rotations would almost certainly induce such terms after electroweak symmetry-breaking. From a purely phenomenological stand-point such mixing must be small in order to avoid constraints from D meson mixing and rare top decays such as $t \rightarrow cZ'^* \rightarrow c\bar{c}c$. We will invoke parameters such that these decays are unobservably small, but they represent a generic feature and an interesting signature that is worthy of further investigation.

⁴There is also direct scattering through the induced coupling to gluons mentioned above, but it leads to predictions well below the current bounds.

4 Dark Matter Annihilation

4.1 Relic Density

In the forbidden channel scenario, the correct relic density can be obtained for DM masses slightly below the mass of the particle running in the loop. For our case this particle is the top quark, favoring dark matter masses between 150 - 170 GeV. While such masses will typically have the correct ballpark relic density, particularly when the annihilation occurs somewhat close to the Z' resonance (~ 350 GeV), the detailed story depends quite sensitively on the entire set of model parameters. For example, annihilation into the 3 body final state tWb can be important (see Fig. 6), especially when the dark matter has sufficient velocity to allow the Wb system to form a close to on-shell top quark. For regions of parameters, processes at the loop level can also be significant. For example, as we will see below, annihilation into Zh is often the most important channel both today and in the early Universe.

In addition, there are viable points for which the Z' is only slightly more heavy than the dark matter and the relic abundance results from annihilation into $Z'Z'$. For example, one has the correct relic abundance for $M'_Z \sim 120$ GeV when $M_\nu = 100$ GeV. Note that the bound on η imposed by direct detection (described in section 3.4) makes the contribution from annihilation via Z - Z' mixing irrelevant for the relic abundance calculation in virtually all of the interesting regions of parameter space.

4.2 One Loop Annihilations and Gamma Ray Lines

At one loop, we have a plethora of final states available as shown in Figures 7 and 8. In addition to line signals from γZ , $\gamma Z'$ and γh , there is potentially an extra line due to the $\gamma\Phi$ channel. Moreover, the one-loop annihilations Zh , $Z'h$, $Z\Phi$, WW , ZZ , ZZ' and $b\bar{b}$ can contribute to a sizable continuum of gamma rays. The analytic results for the effective vertices can be found in the appendices of Ref. [18] and (for annihilation into $b\bar{b}$) appendix A. Annihilation through the Z' - Φ - h , Z' - Φ - Φ and Z' - h - h effective vertices vanishes.

Compared to the original Higgs in Space model [5], there are significantly more one loop diagrams. In that model, $c_L \ll 1$ and only t_R couples to Z' while the T - b - W , t - T - Z , h - T - T and Φ - t - t couplings are suppressed and m_T is large. In the current, UV-complete construction, c_L and c_R are related and go to zero together. In the limit of small mixing between \hat{t}_R and ψ , the t - t - Z' coupling is suppressed and while T has large couplings to both Z and Z' they are both largely vector-like and thus do not contribute [18]. However, there is a new feature in the present work that arises because of the “mixed loops” where both t and T run in the same diagram. The mixed Z' - t - T couplings are less suppressed for small mixing angles and in addition there are enhancements due to the presence of two different mass scales in the loop, leading to a sizable annihilation rate into the vector + a scalar channels, even for modest mixing angles.

To avoid the overwhelming 1-loop annihilations into gluons [37, 43, 44], we focus on the case where DM has vector-like couplings with Z' . Although we are forced to live in a regime of relatively small mixing angles by the EW precision constraints, we can still have large annihilation cross sections into gamma ray lines, as shown in Figures 9, 10 and 11.

In Ref. [18], where no fermion mixing was involved, we found that the dominant channels

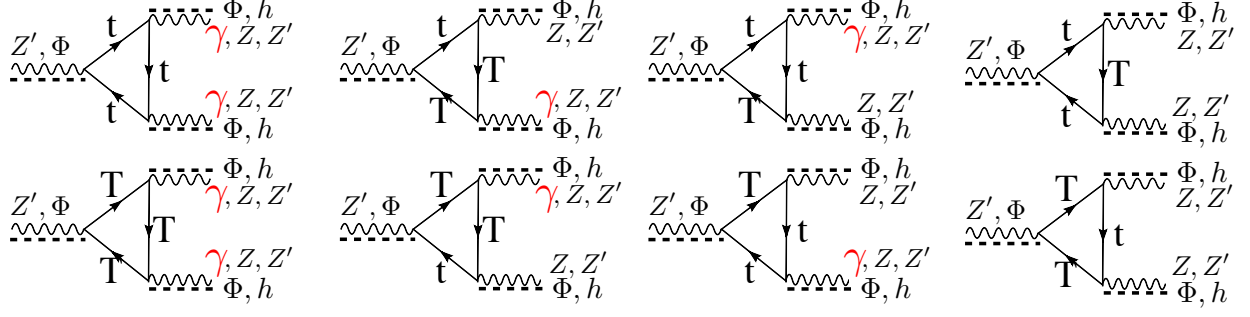


Figure 7: One-loop Z' effective vertices induced by t and T couplings to $\gamma, Z, Z', h, \varphi$.

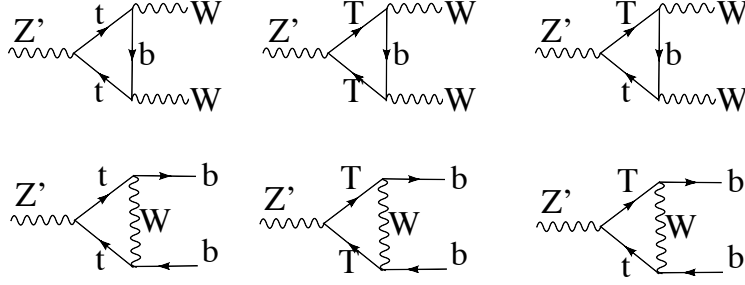


Figure 8: One-loop Z' effective vertices induced by t and T couplings to W .

were $Z\Phi$ and $\gamma\Phi$ ⁵. For the top quark mediator model, we now have the possibility to produce the SM Higgs in the final state. Moreover, because of the presence of “mixed” loops involving both t and T , we find that Zh dominates over γh ⁶ and the discrepancy grows in the limit of small mixing where $g_{tZ'} \ll g_{TZ'}$. In most of the $(y\langle H\rangle, Y\langle\Phi\rangle)$ parameter space, Zh is the dominant annihilation channel, although as shown in Figure 10, there are regions of parameter space where the Zh continuum is relatively suppressed, resulting in a large γZ over continuum ratio.

Roughly speaking, we can classify the situation as to whether the dark matter is heavier or lighter than $(M_Z + M_h)/2$. For the heavier case, the dominant one-loop annihilation channel is Zh . As discussed above, the relic abundance will typically work out for dark matter masses somewhat below the top mass, where there is significant phase space loading of the Zh annihilation rate. Still, a reasonably large line to continuum ratio, as large as $\mathcal{O}(0.1)$ can result, leading to striking line features as illustrated in Fig. 11. In the lighter case, the one-loop continuum tends to be dominated by WW (which is always significantly larger than ZZ due to two very different masses m_t vs. m_b in the loop, leading to some amplitude

⁵This result can be understood as follows: In minimal anomaly-free constructions realizing axial Z' couplings, 1-loop annihilations into two gauge bosons are suppressed due to a cancellation between 1-loop diagrams. Such cancellation does not occur for the $\gamma\Phi$ and $Z\Phi$ channels, which end up dominating.

⁶The “mixed” loops are larger than the top loop, but for the γh channel, they cancel each other exactly as t and T have equal couplings to the photon. Therefore, the γh cross section is entirely controlled by the t loop. On the other hand, for Zh annihilation, the “mixed” loops do not cancel each other, as $g_{tZ} \neq g_{TZ}$, and dominate.

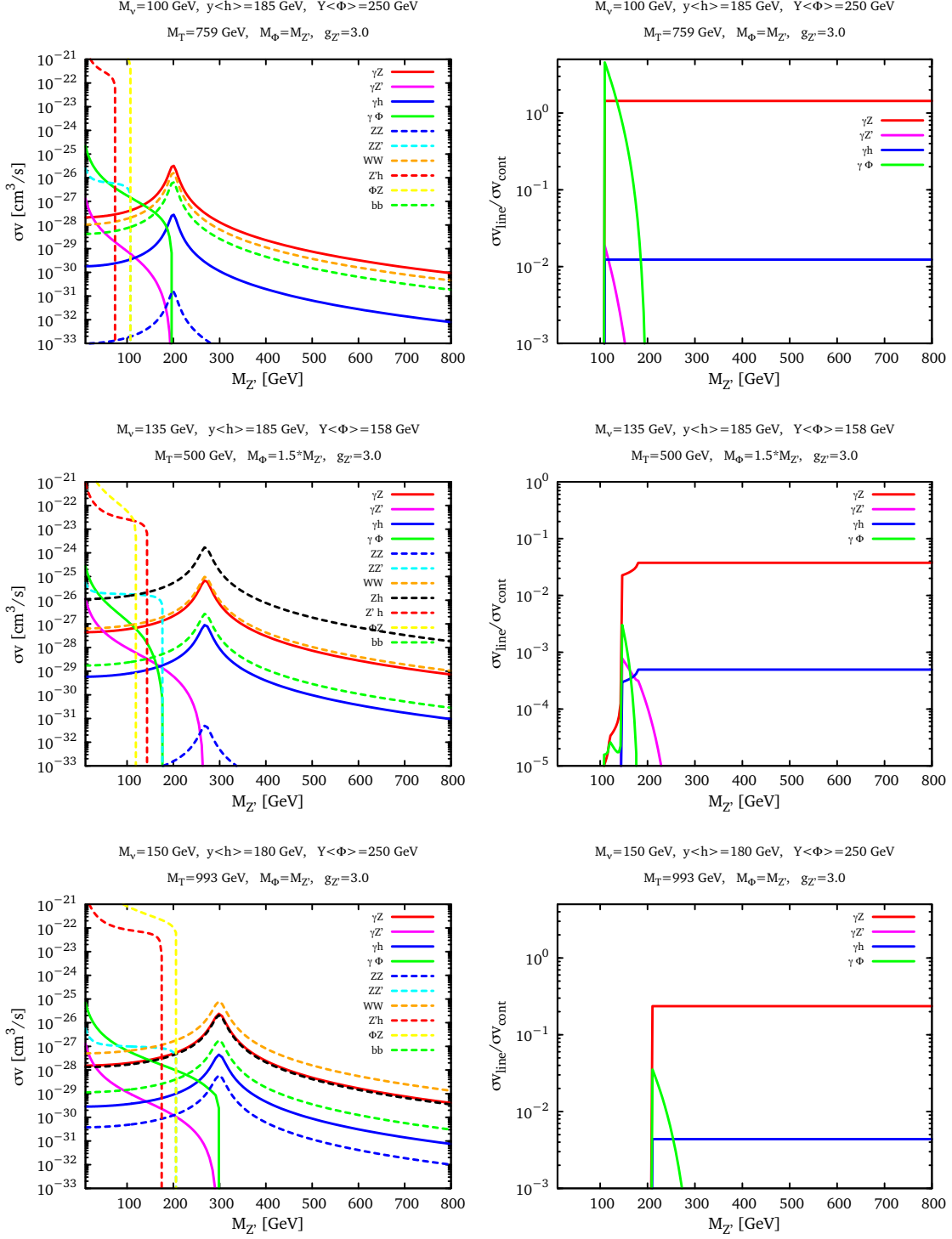


Figure 9: Benchmark predictions for cross sections (as labelled in the plot) and the ratio of line to continuum rates, as a function of the Z' mass. Note that the predictions corresponding to the center panel are essentially unchanged if $M_\nu = 150$ GeV rather than $M_\nu = 135$ GeV, for the same choice of $\langle yH \rangle$ and $\langle Y\Phi \rangle$ values.

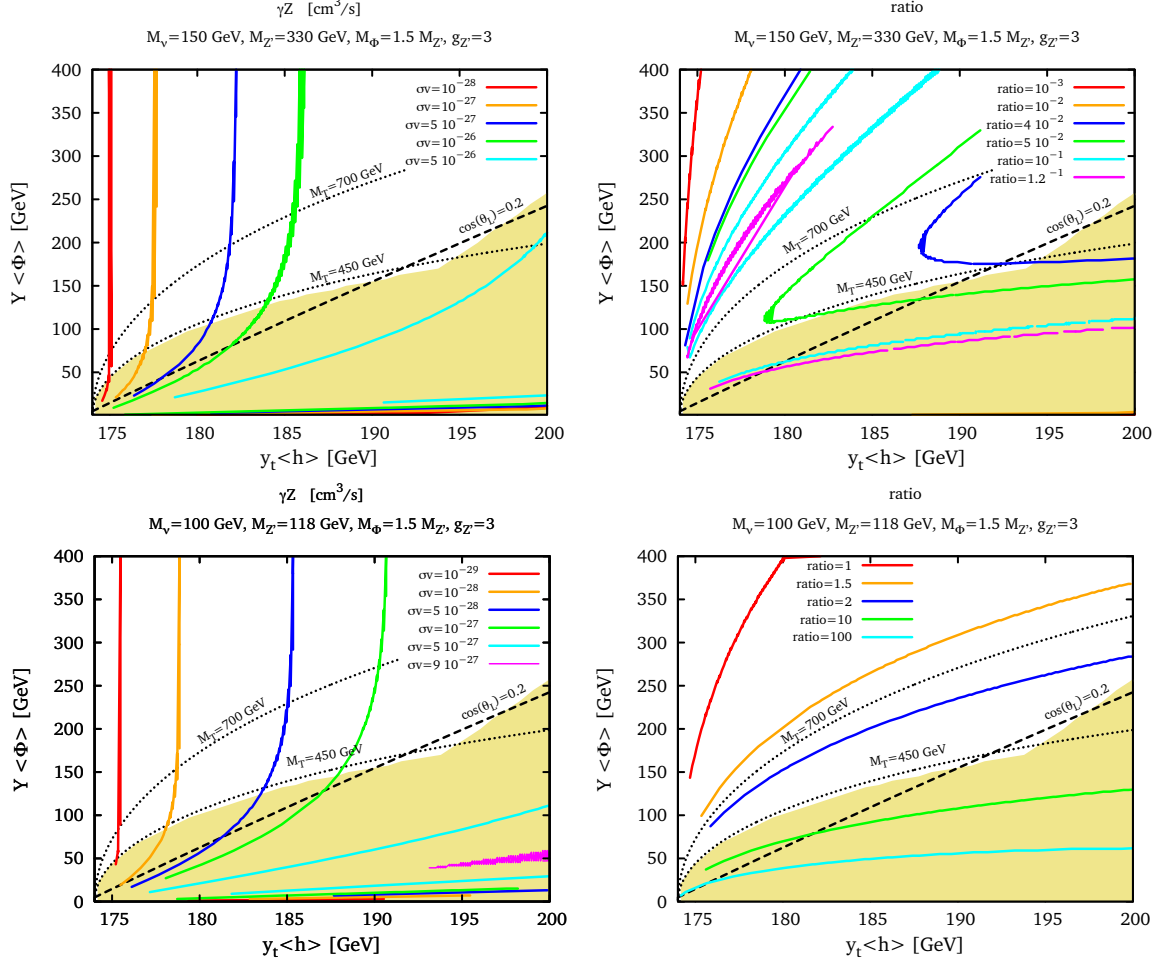


Figure 10: Predictions for line signal rates and ratio to continuum for two choices of DM masses in the plane of $(y\langle H \rangle, Y\langle \Phi \rangle)$. The shaded region is excluded by EW precision tests. In the bottom plots, the choice of the DM and Z' masses guarantees that the correct relic abundance is obtained for essentially the whole plane.

enhancement) which is nonetheless is subdominant to the line annihilation into γZ , resulting in a line to continuum ratio of order one (see Fig. 9). The correct relic abundance can be obtained from annihilation into $Z'Z'$ with $M'_{Z'} \sim 120$ GeV if $M_\nu = 100$ GeV.

Finally, note that a line from annihilation into $\gamma Z'$ is possible, although only for a relatively light Z' which will not typically lead to the correct relic abundance. In addition, there will typically be a very large one-loop continuum contributions from $Z'h$ and/or $Z\Phi$. The $\gamma\Phi$ line may be as intense as the γZ one, however, there is typically a relatively small Z' mass window where $\gamma\Phi$ is kinematically open while $Z\Phi$ is not. When $Z\Phi$ is open, it tends to dominate all channels by several orders of magnitude.

To summarize this section, we find that when the top quark acts as the primary mediator between dark matter and the Standard Model via an s -channel resonance, the dominant line signal tends to be γZ with γh relatively suppressed. The one loop contributions to the continuum annihilation cannot be ignored, and can be dangerously large from annihilation

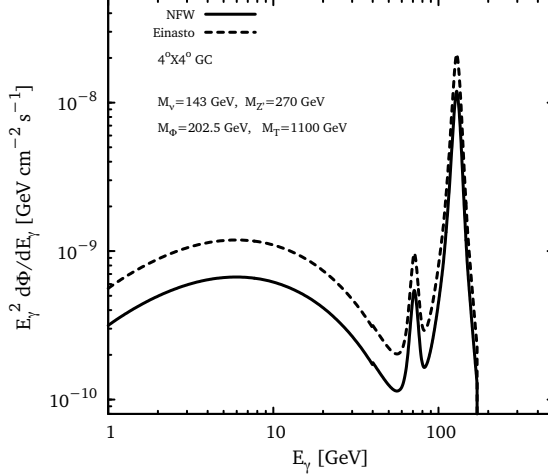


Figure 11: Example of a gamma-ray spectrum obtained for $\langle yH \rangle = 177$ GeV, $\langle Y\Phi \rangle = 200$ GeV, $g_{Z'} = g_{\nu Z'}^V = 3$, leading to a two-line signal at $E_\gamma = 128$ GeV from γZ annihilation with $\sigma_{\gamma Z} v = 2 \times 10^{-27} \text{ cm}^3 \text{ s}^{-1}$ and at $E_\gamma = 71$ GeV from $\gamma \Phi$ annihilation with $\sigma_{\gamma \Phi} v = 1.35 \times 10^{-28} \text{ cm}^3 \text{ s}^{-1}$. The dominant continuum is from WW and Zh annihilations, $\sigma_{WW} v = 5.2 \times 10^{-27} \text{ cm}^3 \text{ s}^{-1}$ and $\sigma_{Zh} v = 1.7 \times 10^{-27} \text{ cm}^3 \text{ s}^{-1}$.

into gg if the dark matter has axial vector interactions, and completely swamp any line signal if $Z\Phi$ is open.

5 An Alternate UV Completion

Large line signals require axial couplings in the loop [18]. The current construction realizes this need by mixing with the SM top quark, making use of its chiral nature, but its effectiveness is limited by the constraints from precision data, which require at most a modest level of mixing. In this Section, we consider a simple extension of the basic UV completion presented above in which the heavy partner fermions ψ have axial couplings with the Z' even before mixing. Consequently, there are large line signals even in the “no-mixing” limit, where the top coupling to the Z' coupling goes to zero (preventing annihilation into $t\bar{t}$), and allowing for dark matter masses well above the top mass.

We start with the previous UV completion of Section 2, and include a second vector-like doublet $\psi_2 = (\psi_{2L}, \psi_{2R}) = (\psi_L^+, \psi_R^-)$ in addition to the original $\psi_1 = (\psi_{1L}, \psi_{1R}) = (\psi_L^-, \psi_R^+)$. Both carry the same SM gauge charges as \hat{t}_R , and ψ_1 also carries $U(1)'$ charge $q_1 = q_\Phi = 1$, whereas ψ_2 has $q_2 = 0$. For simplicity, we set the vector-like masses of ψ_1 and ψ_2 to zero and assume that the Higgs Yukawa coupling between Q_{3L} and ψ_{2R} is negligible. We have Yukawa interactions:

$$\mathcal{L} = y H \bar{Q}_3 \hat{t}_R + Y \Phi \bar{\psi}_L^- \hat{t}_R + \lambda \Phi \bar{\psi}_L^- \psi_R^- + \lambda' \Phi \bar{\psi}_R^+ \psi_R^+ \quad (13)$$

We recycle the formulae Eq. (2–4) for the mass eigenstates t and T , with the replacement that the μ parameter is replaced by $\lambda\langle\Phi\rangle$ in the formula for $\tan\theta_{R/L}$. Imposing that the lightest mass eigenstate has the SM top mass fixes the value of $\mu \equiv \lambda\langle\Phi\rangle$. In addition to

t and T , there is another massive state $T' \equiv \psi^+$ that does not mix with \hat{t}_R and which has mass given by $M_{T'} = \lambda' \langle \Phi \rangle$. In this way, we realize the existence of two massive states T and T' with axial-vector couplings to the Z' , even in the limit that the SM top quark is purely unmixed.

With respect to the previous case, the couplings to the Z' and Φ are modified, whereas the couplings to the Z and SM Higgs are not. In particular, t_R no longer couples to the Z' . The modified couplings can be summarized:

$$g_{ttZ'}^V = \frac{g_{Z'}}{2} c_L^2, \quad g_{ttZ'}^A = -\frac{g_{Z'}}{2} c_L^2, \quad g_{TTZ'}^V = \frac{g_{Z'}}{2} s_L^2, \quad g_{TTZ'}^A = -\frac{g_{Z'}}{2} s_L^2, \quad (14)$$

$$g_{tTZ'}^V = \frac{g_{Z'}}{2} c_L s_L, \quad g_{tTZ'}^A = -\frac{g_{Z'}}{2} c_L s_L, \quad (15)$$

$$y_{tt\Phi}^S = -Y c_L s_R + \lambda c_L c_R, \quad y_{TT\Phi}^S = Y s_L c_R + \lambda s_L s_R, \quad y_{tt\Phi}^P = 0, \quad y_{TT\Phi}^P = 0 \quad (16)$$

$$y_{tT\Phi}^S = \frac{1}{2}[Y(c_L c_R - s_L s_R) + \lambda(c_L s_R + s_L c_R)], \quad y_{tT\Phi}^P = \frac{1}{2}[Y(c_L c_R + s_L s_R) + \lambda(c_L s_R - s_L c_R)] \quad (17)$$

and in addition

$$g_{T'T'Z'}^V = \frac{g_{Z'}}{2}, \quad g_{T'T'Z'}^A = \frac{g_{Z'}}{2}, \quad (18)$$

$$y_{T'T'\Phi}^S = \lambda', \quad y_{T'T'\Phi}^P = 0 \quad (19)$$

To simplify the parameter space, we set all pseudo scalar couplings of ψ to Φ in the Lagrangian to zero, although the mass eigenstates end up with pseudo-scalar couplings for the Φ - t - T vertex. Having set the DM pseudo-scalar couplings to zero, the one-loop diagrams mediated by Φ will be p -wave suppressed, leaving the relevant contributions from Z' exchange.

As mentioned above, this framework evades large annihilation into $t\bar{t}$ when the dark matter mass is above the top mass. However, because the constraints from precision measurements are greatly relaxed, T and T' can as light as the direct search bounds of ~ 475 GeV, and one can obtain the correct relic abundance from annihilation into $t\bar{T}/T\bar{t}$, $T\bar{T}$, $T'\bar{T}'$ or $Z'\Phi$. One-loop DM annihilations are dominated by the contributions of T and T' , although mixed (t, T) loops still play an important role. Zh dominates the continuum when it is kinematically accessible.

There are line signals from γZ , $\gamma Z'$ and $\gamma\Phi$, whose relative sizes depend on the choice of parameters, in particular the relative masses of ν , Z' and Φ . We illustrate some cross section predictions in Figs. 12 and 13. Typically, we find that the dominant line is due to $\gamma\Phi$. In the scan plots of Fig. 13, we therefore show contours for $\sigma_{\gamma\Phi} v$ and the ratio $\sigma_{\gamma\Phi} v$ over continuum, finding that the value of $\sigma_{\gamma\Phi} v$ is essentially constant in the plane $\langle yH \rangle, \langle Y\Phi \rangle$, as it is nearly independent of the mixing angles. However, the other channels depend very sensitively on them. As a result, the line over continuum ratios range over several orders of magnitude depending on where in the plane one considers. In Fig. 14, we show an illustrative 2-peak spectrum due to $M_\nu = 500$ GeV DM annihilation into $\gamma\Phi$ and $\gamma Z'$.

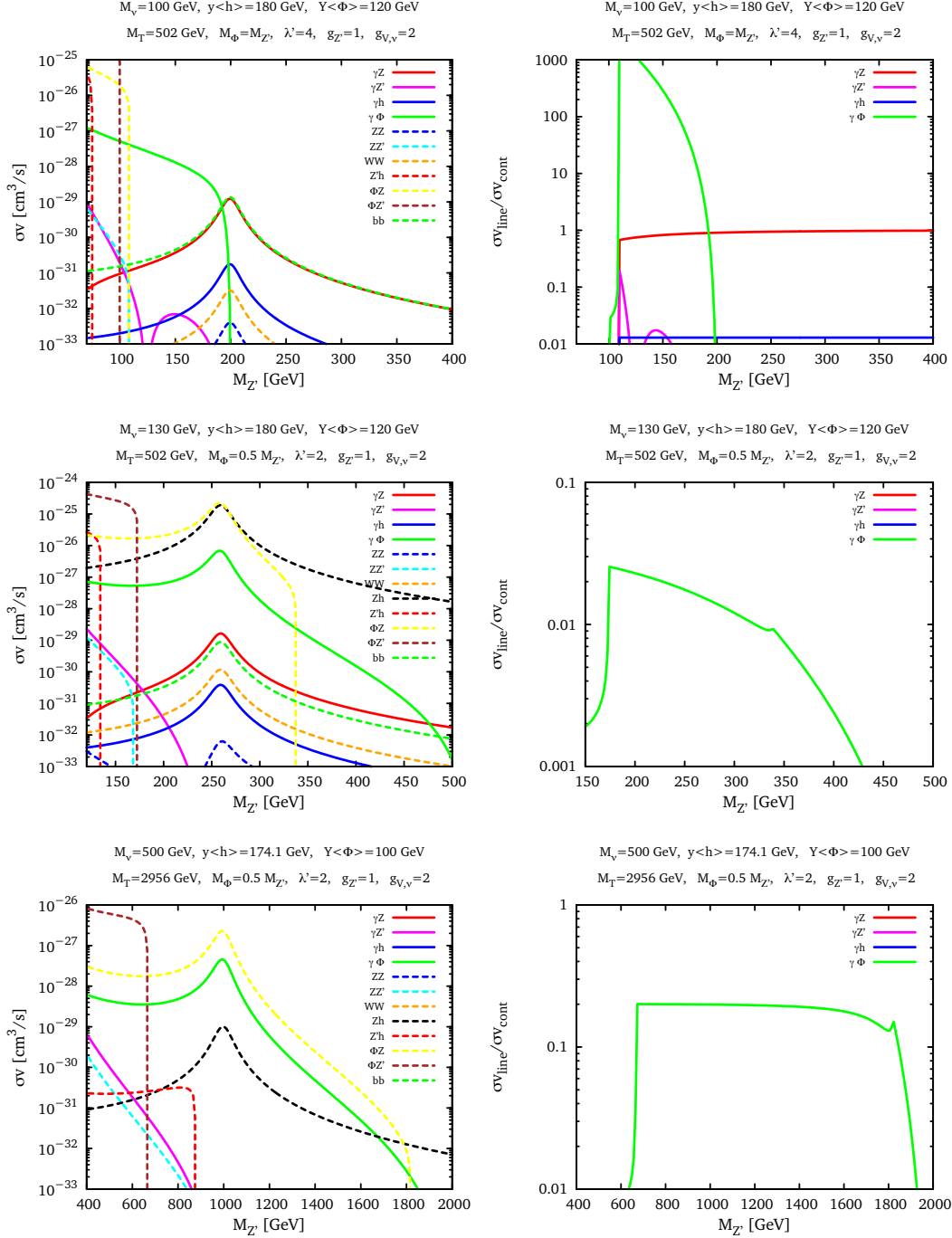


Figure 12: Predictions for cross sections and line to continuum ratios in the second UV completion. The upper plot corresponds to a light DM case where the $\gamma\Phi$ line signal is huge and the continuum is essentially absent for Z' masses leading to the correct relic abundance. The center plots are quite typical of what happens for a generic choice of parameter, with Zh and $Z\Phi$ channels dominating. The lower plots correspond to the case where $\langle yH \rangle \rightarrow m_t$ and mixing angles vanish. In this situation $Z\Phi$ and $\gamma\Phi$ are the main channels [18].

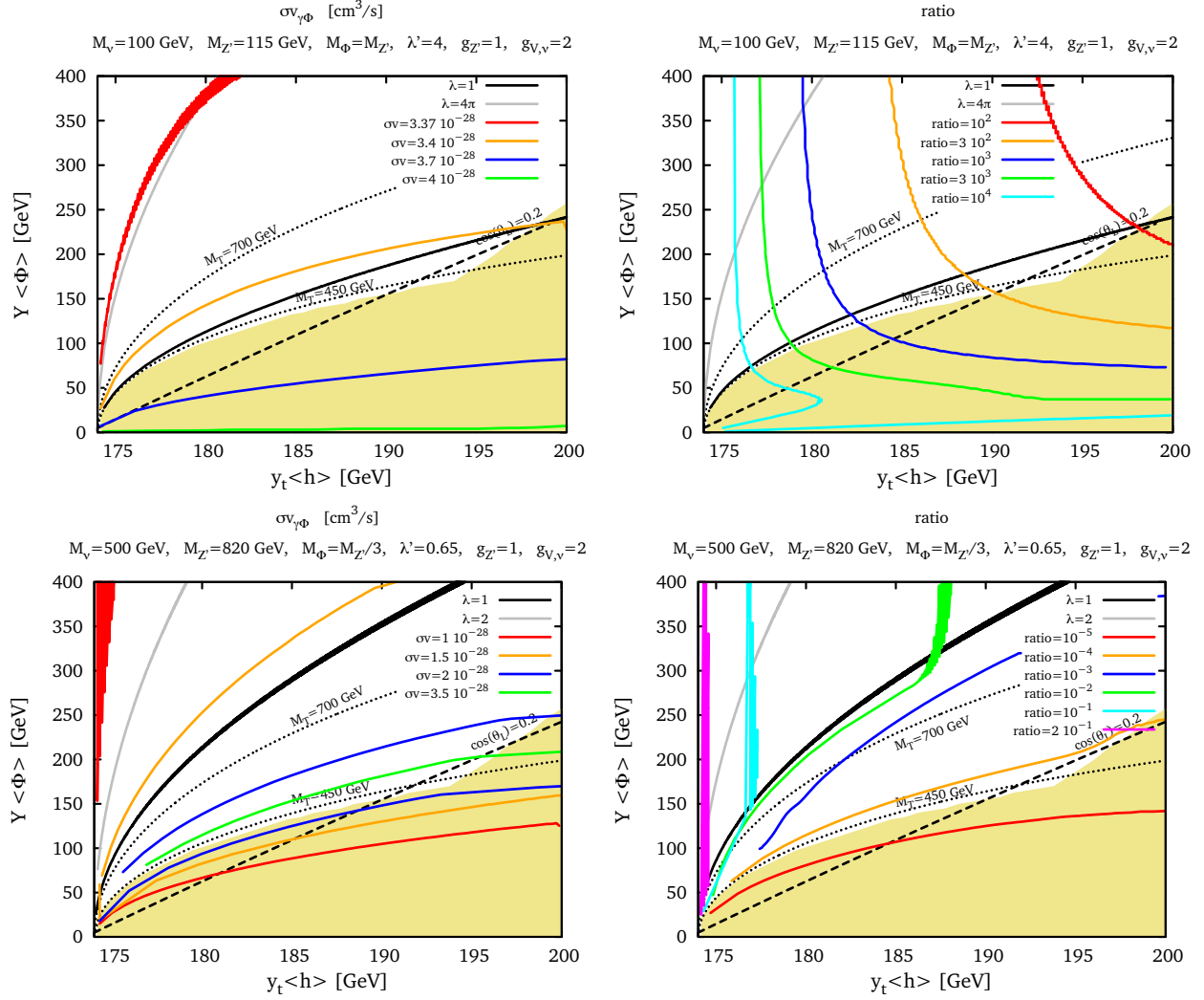


Figure 13: Predictions in the second UV completion, scanning over the plane of $y\langle h\rangle$ - $Y\langle\Phi\rangle$, where the shaded region is excluded by EW precision tests. In the upper plots, the choice of the DM and Z' masses guarantees that the correct relic abundance is recovered in the whole plane through $\nu\bar{\nu} \rightarrow Z'Z'$. For the lower plots, the relic abundance is controlled by annihilation into $T'T'$ ($M_{T'} \sim 530$ GeV), $Z'\Phi$ or tT in the region $M_T \lesssim 800$ GeV, in the early Universe, with the correct relic abundance recovered in a significant fraction of the $(\langle yH\rangle, \langle Y\Phi\rangle)$ plane, (particularly in the region where the line over continuum ratio is larger than 10^{-2}).

6 Summary

We have considered a class of models where the dark matter is a Dirac fermion whose connection with the Standard Model is primarily through the Top quark. We considered two variations of UV complete models, and found that both lead to large gamma-ray line signatures from annihilation into either γZ or $\gamma\Phi$, where Φ is the scalar responsible for the breaking of a new $U(1)'$ gauge symmetry. In the first variant, the Z' has sizable coupling to the top quark and a mass only slightly below it, realizing the forbidden channel mechanism

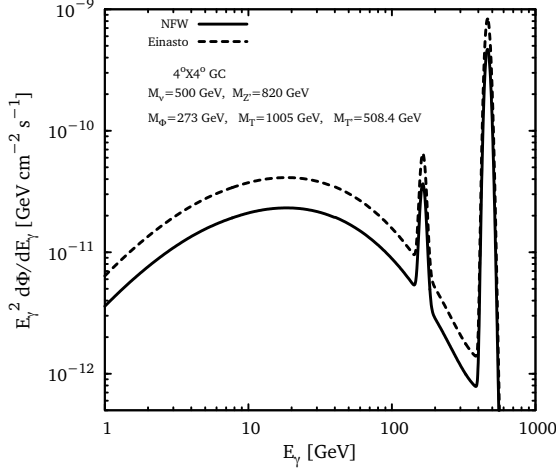


Figure 14: Example of a gamma-ray spectrum obtained in the second UV completion for $\langle yH \rangle = 174.6$ GeV, $Y = 0.1$, $\lambda' = 0.62$, $g_{Z'} = 1 = g_{\nu Z'}^V/2$, leading to a two-line signal at $E_\gamma = 164$ GeV from $\gamma Z'$ annihilation with $\sigma_{\gamma Z'} v = 4 \times 10^{-29} \text{ cm}^3 \text{ s}^{-1}$ and at $E_\gamma = 463$ GeV from $\gamma \Phi$ annihilation with $\sigma_{\gamma \Phi} v = 2 \times 10^{-28} \text{ cm}^3 \text{ s}^{-1}$. The dominant continuum is from $Z\Phi$ annihilations, $\sigma_{Z\Phi} v = 5 \times 10^{-28} \text{ cm}^3 \text{ s}^{-1}$. Relic abundance is controlled by $\nu \bar{\nu} \rightarrow T' T'$ which is open in the early universe but not today.

by which the dark matter annihilates primarily into top quarks in the early universe, but this annihilation is shut off for cold dark matter particles today. In the second UV completion, the Z' coupling to top quarks is very suppressed, and the dark matter mass can be much larger than the top mass. In both cases, Zh (and, depending on the Φ mass, $Z\Phi$) is typically the dominant annihilation channel, illustrating the need to carefully consider one-loop contributions to the continuum photons in theories with enhanced line signals.

Gamma ray line signatures are an important item on the menu of indirect searches for dark matter. Models such as the ones considered here, which suppress the continuum from annihilations today, are particularly well-probed by these searches. What is perhaps more surprising is the fact that these models are surprisingly immune to constraints from the LHC and direct detection as well, which would suggest that the gamma ray sky hides unique probes of interesting dark theories.

Acknowledgments

G. Servant is supported by the ERC starting grant Cosmo@LHC (204072). G. Shaughnessy is supported by the U. S. Department of Energy under the contract DE-FG-02-95ER40896. T. Tait acknowledges the hospitality of the SLAC theory group, and is supported in part by NSF grant PHY-0970171. He also thanks P. Fox, J. Kearny, and A. Pierce for early collaboration and discussions, and the Aspen Center for Physics, under NSF Grant No. 1066293, where part of this work was completed. The work of M. Taoso is supported by the European Research Council (ERC) under the EU Seventh Framework Programme (FP7/2007-2013) / ERC Starting Grant (agreement n. 278234 - ‘NewDark’ project).

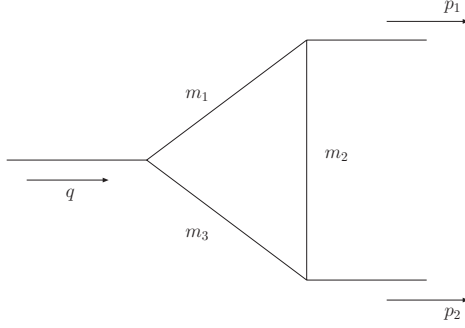


Figure 15: Topology for the effective vertices.

A One-loop annihilation into $b\bar{b}$

In this appendix, we summarize the one-loop expressions for the effective vertex and amplitudes-squared needed for the $b\bar{b}$ channel. One-loop expressions for all other channels are listed in the appendix of Ref. [18]. The topology for the loop diagrams considered here is shown in Fig. 15. We express the amplitude in terms of two-point (B_0) and three-point (C_0) scalar integrals where:

$$C_0 = C_0(M_1^2, M_2^2, 4M_\nu^2; m_1^2, m_2^2, m_3^2), \quad (20)$$

$$B_0(23) = B_0(M_2^2; m_2^2, m_3^2), \quad (21)$$

$$B_0(13) = B_0(4M_\nu^2; m_1^2, m_3^2), \quad (22)$$

$$B_0(12) = B_0(M_1^2; m_1^2, m_2^2). \quad (23)$$

In the following expressions, $m_1 = m_3 \equiv m_f$ and $m_2 = M_W$. However, to derive our results, we have computed all of the expressions in these appendices in terms of the general masses as depicted in Fig. 15.

The effective vertex for $Z'^\alpha \rightarrow b\bar{b}$ is given by the expression:

$$\mathcal{V}_{Z' \rightarrow b\bar{b}}^\alpha = A \bar{u}(p_1) \gamma^\alpha (1 - \gamma_5) v(p_2), \quad (24)$$

where the loop coefficient A is:

$$\begin{aligned}
A = & \frac{(g_{f\bar{b}}^W)^2}{32\pi^2 M_\nu^2 M_W^2} \left(8A_0(m_f)M_\nu^2(a_{f\bar{f}}^{Z'} - v_{f\bar{f}}^{Z'}) - m_f^4 \left((a_{f\bar{f}}^{Z'} + v_{f\bar{f}}^{Z'})(B_0(12) + B_0(13) \right. \right. \\
& - 2B_0(23)) + 8C_0M_\nu^2(v_{f\bar{f}}^{Z'} - a_{f\bar{f}}^{Z'}) \left. \left. - 2M_W^4 \left((a_{f\bar{f}}^{Z'} - v_{f\bar{f}}^{Z'}) \left(B_0(12) + B_0(13) \right. \right. \right. \right. \\
& - 2 \left(B_0(23) + 8C_0M_\nu^2 \right) \left. \left. \right) + C_0m_f^2(5a_{f\bar{f}}^{Z'} - 3v_{f\bar{f}}^{Z'}) \right) + M_W^2 \left(m_f^2(3a_{f\bar{f}}^{Z'} - v_{f\bar{f}}^{Z'}) \left(B_0(12) \right. \right. \\
& + B_0(13) - 2 \left(B_0(23) + 8C_0M_\nu^2 \right) \left. \left. \right) + 8M_\nu^2(a_{f\bar{f}}^{Z'} - v_{f\bar{f}}^{Z'}) \left(-2B_0(12) - B_0(13) + 3B_0(23) \right. \right. \\
& + 8C_0M_\nu^2 + 1 \left. \left. \right) + 8C_0a_{f\bar{f}}^{Z'}m_f^4 \right) + 4M_\nu^2m_f^2(a_{f\bar{f}}^{Z'}(2B_0(12) + B_0(23) - 1) + v_{f\bar{f}}^{Z'}(-2B_0(12) \\
& + B_0(23) - 1)) - 2C_0m_f^6(a_{f\bar{f}}^{Z'} + v_{f\bar{f}}^{Z'}) + 4C_0M_W^6(a_{f\bar{f}}^{Z'} - v_{f\bar{f}}^{Z'}) \left. \right). \tag{25}
\end{aligned}$$

The matrix-element-squared takes the form:

$$|\mathcal{M}|^2 = \frac{N_c}{4} \frac{M_\nu^4}{|\Sigma_{Z'}|^2} \left(\frac{(a_{\nu\bar{\nu}}^{Z'})^2 m_b^2 (M_{Z'}^2 - 4M_\nu^2)^2}{4M_\nu^2 M_{Z'}^4} + (v_{\nu\bar{\nu}}^{Z'})^2 \right) \tag{26}$$

B $t\bar{t}$ production mediated by Z'

In this appendix, we provide the expressions for Z' production at the LHC. The Z' is produced via loop coupling to gluon pairs through the top sector. Similar to the $Z'\gamma\gamma$ process, the $Z'gg$ vertex convention is shown in Fig. 16 and is given by [18]

$$\mathcal{V}_{ggZ'}^{\mu\nu\alpha} = \Gamma_{ggZ'}^{\mu\nu\alpha} \delta^{ab} \sum_f \frac{N_c^f g_s^2 a_{f\bar{f}}}{4\pi^2} (1 + 2m_f^2 C_0(M_{Z'}^2, 0, 0, m_f^2, m_f^2, m_f^2)), \tag{27}$$

where N_c^f is the color factor of the internal fermion, g_s is the $SU(3)$ coupling, $a_{f\bar{f}}$ is the axial-vector $Z' - f - f$ coupling. The tensor structure of the ggZ' vertex is given by

$$\Gamma_{ggZ'}^{\mu\nu\alpha} = \epsilon^{p_1\mu\nu\alpha} - \epsilon^{p_2\mu\nu\alpha} + \frac{p_2^\mu \epsilon^{p_1 p_2 \nu \alpha} - p_1^\nu \epsilon^{p_1 p_2 \mu \alpha}}{2M_{Z'}^2} \tag{28}$$

The loop function C_0 can be reduced in this instance to

$$C_0(M_{Z'}^2, 0, 0, m_f^2, m_f^2, m_f^2) = \frac{1}{2M_{Z'}^2} \log^2 \left(\frac{\beta_f - 1}{\beta_f + 1} \right), \tag{29}$$

where $\beta_f = \sqrt{1 - \frac{4m_f^2}{M_{Z'}^2}}$. Thus, the effective vertex becomes

$$\mathcal{V}_{ggZ'}^{\mu\nu\alpha} = \Gamma_{ggZ'}^{\mu\nu\alpha} \delta^{ab} \sum_f \frac{N_c^f g_s^2 a_{f\bar{f}}}{4\pi^2} \left(1 + \frac{m_f^2}{M_{Z'}^2} \log^2 \left(\frac{\beta_f - 1}{\beta_f + 1} \right) \right), \tag{30}$$

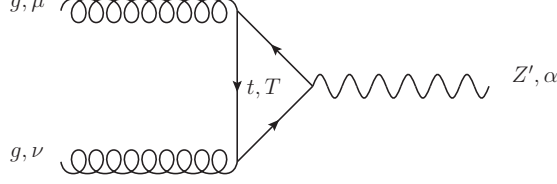


Figure 16: Effective $Z'gg$ vertex mediated through t and T loops.

The Landau-Yang theorem forces a vanishing vertex when any of the external bosons is on-shell. Therefore, the leading production mechanism of the Z' is in association with a gluon or quark shown in Fig. 5. The Z' subsequently decays to $t\bar{t}$ pairs.

The amplitude for $g(q_1) + g(q_2) \rightarrow t(p_t) + \bar{t}(p'_t)$ can be expressed as:

$$\mathcal{M}_{gg \rightarrow Z' \rightarrow t\bar{t}} = \bar{u}(p_t) \gamma^\beta \left(v_{tt}^{Z'} + a_{tt}^{Z'} \gamma_5 \right) v(p'_t) \frac{\left(-g_{\alpha\beta} + \frac{p_{Z',\alpha} p_{Z',\beta}}{M_{Z'}^2} \right)}{(q_1 + q_2)^2 - M_{Z'}^2 + i M_{Z'} \Gamma_{Z'}} A \Gamma_{ggZ'}^{\mu\nu\alpha} \epsilon(q_1)_\mu \epsilon(q_2)_\nu \quad (31)$$

where we have expressed the $Z'gg$ vertex as $\mathcal{V}_{Z'gg} = A \Gamma_{ggZ'}^{\mu\nu\alpha}$ and $\epsilon(q_1)_\mu$ and $\epsilon(q_2)_\nu$ are the polarization tensors of the incoming gluons. Note that when we square this amplitude and average over the gluon polarizations $\epsilon(q_1)_\mu$ and $\epsilon(q_2)_\nu$, we must do so in such a way that only the physical (transverse) polarization states contribute to the matrix-element-squared. To do this we adopt the general prescription:

$$\sum_{\lambda_i=1,2} \epsilon_\mu(q_i, \lambda_i) \epsilon_{\mu'}^*(q_i, \lambda_i) = -g_{\mu\mu'} + \frac{n_{i\mu} q_{i\mu'} + q_{i\mu} n_{i\mu'}}{n_i \cdot q_i} - \frac{n_i^2 q_{i\mu} q_{i\mu'}}{(n_i \cdot q_i)^2}, \quad (32)$$

where $i = 1, 2$ and the arbitrary vectors n_i have to satisfy the relations:

$$n_i^\mu \sum_{\lambda=1,2} \epsilon_\mu(q_i, \lambda_i) \epsilon_{\mu'}^*(q_i, \lambda_i) = 0, \quad n_i^{\mu'} \sum_{\lambda=1,2} \epsilon_\mu(q_i, \lambda_i) \epsilon_{\mu'}^*(q_i, \lambda_i) = 0 \quad (33)$$

together with $n_i^2 \neq 0$ and $n_1 \neq n_2$. We choose $n_1 = q_2$ and $n_2 = q_1$ such that:

$$\sum_{\lambda_i=1,2} \epsilon_\mu(q_i, \lambda_i) \epsilon_{\mu'}^*(q_i, \lambda_i) = -g_{\mu\mu'} + 2 \frac{q_{1\mu} q_{2\mu'} + q_{2\mu} q_{1\mu'}}{s}, \quad (34)$$

where $s = (q_1 + q_2)^2$.

Finally, summing over the final-state top quark polarizations and averaging over the initial state gluon polarizations, we find for the matrix-element-squared:

$$\overline{\sum |\mathcal{M}|^2} = \frac{(a_{tt}^{Z'})^2 m_t^2 |A|^2 s}{32 ((s - M_{Z'}^2)^2 + M_{Z'}^2 \Gamma_{Z'}^2)} \left[1 - \frac{s}{M_{Z'}^2} \right]^2. \quad (35)$$

We see that in the limit where the Z' goes on-shell ($s \rightarrow M_{Z'}^2$) the amplitude-squared vanishes in accordance to the Landau-Yang theorem.

References

- [1] M. Ackermann *et al.* [Fermi-LAT Collaboration], Phys. Rev. Lett. **107**, 241302 (2011) [arXiv:1108.3546 [astro-ph.HE]].
- [2] M. Ackermann *et al.* [LAT Collaboration], Phys. Rev. D **86**, 022002 (2012) [arXiv:1205.2739 [astro-ph.HE]].
- [3] S. D. McDermott, H. -B. Yu and K. M. Zurek, Phys. Rev. D **83**, 063509 (2011) [arXiv:1011.2907 [hep-ph]].
- [4] G. Steigman, B. Dasgupta and J. F. Beacom, Phys. Rev. D **86**, 023506 (2012) [arXiv:1204.3622 [hep-ph]].
- [5] C. B. Jackson, G. Servant, G. Shaughnessy, T. M. P. Tait and M. Taoso, JCAP **1004**, 004 (2010) [arXiv:0912.0004 [hep-ph]].
- [6] K. Agashe and G. Servant, Phys. Rev. Lett. **93**, 231805 (2004) [hep-ph/0403143].
- [7] K. Agashe and G. Servant, JCAP **0502**, 002 (2005) [hep-ph/0411254].
- [8] E. Dudas, Y. Mambrini, S. Pokorski and A. Romagnoni, JHEP **0908**, 014 (2009) [arXiv:0904.1745 [hep-ph]]; Y. Mambrini, JCAP **0912**, 005 (2009) [arXiv:0907.2918 [hep-ph]]; E. Dudas, Y. Mambrini, S. Pokorski and A. Romagnoni, arXiv:1205.1520 [hep-ph]; M. R. Buckley and D. Hooper, Phys. Rev. D **86**, 043524 (2012) [arXiv:1205.6811 [hep-ph]]; Z. Kang, T. Li, J. Li and Y. Liu, arXiv:1206.2863 [hep-ph]; S. Tulin, H. -B. Yu and K. M. Zurek, arXiv:1208.0009 [hep-ph]; Y. Bai and J. Shelton, JHEP **1212**, 056 (2012) [arXiv:1208.4100 [hep-ph]]; H. M. Lee, M. Park and W. -I. Park, JHEP **1212**, 037 (2012) [arXiv:1209.1955 [hep-ph]]; N. Bernal, C. Boehm, S. Palomares-Ruiz, J. Silk and T. Toma, arXiv:1211.2639 [hep-ph]; H. M. Lee, M. Park and V. Sanz, arXiv:1212.5647 [hep-ph]; J. Kopp, E. T. Neil, R. Primulando and J. Zupan, arXiv:1301.1683 [hep-ph]; J. Fan and M. Reece, arXiv:1301.2597 [hep-ph].
- [9] C. Weniger, JCAP **1208**, 007 (2012) [arXiv:1204.2797 [hep-ph]].
- [10] E. Tempel, A. Hektor and M. Raidal, JCAP **1209**, 032 (2012) [Addendum-ibid. **1211**, A01 (2012)] [arXiv:1205.1045 [hep-ph]].
- [11] M. Su and D. P. Finkbeiner, arXiv:1206.1616 [astro-ph.HE].
- [12] K. Rao and D. Whiteson, arXiv:1210.4934 [astro-ph.HE].
- [13] A. Rajaraman, T. M. P. Tait and D. Whiteson, JCAP **1209**, 003 (2012) [arXiv:1205.4723 [hep-ph]].
- [14] T. Cohen, M. Lisanti, T. R. Slatyer and J. G. Wacker, JHEP **1210**, 134 (2012) [arXiv:1207.0800 [hep-ph]].
- [15] D. P. Finkbeiner, M. Su and C. Weniger, JCAP **1301**, 029 (2013) [arXiv:1209.4562 [astro-ph.HE]].

- [16] A. Hektor, M. Raidal and E. Tempel, arXiv:1209.4548 [astro-ph.HE].
- [17] D. Whiteson, JCAP **1211**, 008 (2012) [arXiv:1208.3677 [astro-ph.HE]].
- [18] C. B. Jackson, G. Servant, G. Shaughnessy, T. M. P. Tait and M. Taoso, arXiv:1302.1802 [hep-ph].
- [19] M. S. Carena, A. Daleo, B. A. Dobrescu and T. M. P. Tait, Phys. Rev. D **70**, 093009 (2004) [hep-ph/0408098].
- [20] B. A. Dobrescu and C. T. Hill, Phys. Rev. Lett. **81**, 2634 (1998) [hep-ph/9712319].
- [21] R. S. Chivukula, B. A. Dobrescu, H. Georgi and C. T. Hill, Phys. Rev. D **59**, 075003 (1999) [hep-ph/9809470].
- [22] H. -J. He, T. M. P. Tait and C. P. Yuan, Phys. Rev. D **62**, 011702 (2000) [hep-ph/9911266].
- [23] H. -J. He, C. T. Hill and T. M. P. Tait, Phys. Rev. D **65**, 055006 (2002) [hep-ph/0108041].
- [24] M. E. Peskin and T. Takeuchi, Phys. Rev. D **46**, 381 (1992).
- [25] S. Dawson and E. Furlan, arXiv:1205.4733 [hep-ph].
- [26] M. Baak, M. Goebel, J. Haller, A. Hoecker, D. Kennedy, R. Kogler, K. Moenig and M. Schott *et al.*, Eur. Phys. J. C **72**, 2205 (2012) [arXiv:1209.2716 [hep-ph]].
- [27] K. Rao and D. Whiteson, arXiv:1204.4504 [hep-ph].
- [28] S. Chatrchyan *et al.* [CMS Collaboration], arXiv:1203.5410 [hep-ex].
- [29] G. Aad *et al.* [ATLAS Collaboration], arXiv:1207.7214 [hep-ex]; S. Chatrchyan *et al.* [CMS Collaboration], [arXiv:1207.7235 [hep-ex]].
- [30] A. Djouadi, M. Spira and P. M. Zerwas, Phys. Lett. B **264**, 440 (1991).
- [31] L. D. Landau, Dokl. Akad. Nauk., USSR **60**, 207 (1948); C. N. Yang, Phys. Rev. **77**, 242 (1950).
- [32] J. Alwall, M. Herquet, F. Maltoni, O. Mattelaer and T. Stelzer, JHEP **1106**, 128 (2011) [arXiv:1106.0522 [hep-ph]].
- [33] M. Beltran, D. Hooper, E. W. Kolb, Z. A. C. Krusberg and T. M. P. Tait, JHEP **1009**, 037 (2010) [arXiv:1002.4137 [hep-ph]]; J. Goodman, M. Ibe, A. Rajaraman, W. Shepherd, T. M. P. Tait and H. -B. Yu, Phys. Lett. B **695**, 185 (2011) [arXiv:1005.1286 [hep-ph]]; J. Goodman, M. Ibe, A. Rajaraman, W. Shepherd, T. M. P. Tait and H. -B. Yu, Phys. Rev. D **82**, 116010 (2010) [arXiv:1008.1783 [hep-ph]]; A. Rajaraman, W. Shepherd, T. M. P. Tait and A. M. Wijangco, Phys. Rev. D **84**, 095013 (2011) [arXiv:1108.1196 [hep-ph]]; P. J. Fox, R. Harnik, J. Kopp and Y. Tsai, Phys. Rev. D **85**, 056011 (2012) [arXiv:1109.4398 [hep-ph]].

- [34] G. Aad *et al.* [ATLAS Collaboration], arXiv:1210.4491 [hep-ex].
- [35] Y. Bai, P. J. Fox and R. Harnik, JHEP **1012**, 048 (2010) [arXiv:1005.3797 [hep-ph]]; I. M. Shoemaker and L. Vecchi, Phys. Rev. D **86**, 015023 (2012) [arXiv:1112.5457 [hep-ph]]; H. An, X. Ji and L. -T. Wang, JHEP **1207**, 182 (2012) [arXiv:1202.2894 [hep-ph]]; M. T. Frandsen, F. Kahlhoefer, A. Preston, S. Sarkar and K. Schmidt-Hoberg, JHEP **1207**, 123 (2012) [arXiv:1204.3839 [hep-ph]].
- [36] H. M. Lee, M. Park and V. Sanz, arXiv:1212.5647 [hep-ph].
- [37] K. Cheung, K. Mawatari, E. Senaha, P. -Y. Tseng and T. -C. Yuan, JHEP **1010**, 081 (2010) [arXiv:1009.0618 [hep-ph]].
- [38] G. Bevilacqua and M. Worek, JHEP **1207**, 111 (2012) [arXiv:1206.3064 [hep-ph]].
- [39] B. Lillie, J. Shu and T. M. P. Tait, JHEP **0804**, 087 (2008) [arXiv:0712.3057 [hep-ph]]; K. Kumar, T. M. P. Tait and R. Vega-Morales, JHEP **0905**, 022 (2009) [arXiv:0901.3808 [hep-ph]].
- [40] A. Pomarol and J. Serra, Phys. Rev. D **78** (2008) 074026 [arXiv:0806.3247 [hep-ph]].
- [41] G. Servant, DESY-PROC-2010-01; L. Gauthier, PhD thesis, 2012, IRFU-12-05-T; L. Gauthier, R. Kukla and G. Servant, in preparation.
- [42] E. Aprile *et al.* [XENON100 Collaboration], Phys. Rev. Lett. **109**, 181301 (2012) [arXiv:1207.5988 [astro-ph.CO]].
- [43] X. Chu, T. Hambye, T. Scarna and M. H. G. Tytgat, Phys. Rev. D **86**, 083521 (2012) [arXiv:1206.2279 [hep-ph]].
- [44] Y. Zhang, Phys. Lett. B **720**, 137 (2013) [arXiv:1212.2730 [hep-ph]].